Journal of Materials Chemistry B

PAPER

View Article Online
View Journal | View Issue

Cite this: J. Mater. Chem. B, 2015, 3, 1957

Super LCST thermo-responsive nanoparticle assembly for ATP binding through the Hofmeister effect†

Smita Kashyap‡ and Manickam Jayakannan‡*

Received 8th November 2014
Accepted 12th January 2015

DOI: 10.1039/c4tb01844c

www.rsc.org/MaterialsB

The present investigation reports the development of a super LCST thermo-responsive amphiphilic nanoparticle assembly for the detection of adenosine triphosphate (ATP) through the Hofmeister effect. For this purpose, a new diblock molecule was designed based on hydrophilic polyethylene glycol and the renewable resource 3-pendadecylphenol as the hydrophobic unit. The amphiphile self-assembled as a 150 nm micellar nanoparticle and showed a super lower critical solution temperature (LCST) above 90 °C. The amphiphile followed the Hofmeister effect for the anion series and exhibited high selectivity for the recognition of ATP over its adenosine precursors such as ADP, AMP and inorganic phosphate (Pi). The preferential binding for ATP is attributed to the encapsulation in the hydrophobic pocket and modification of the hydration shell at the periphery of the amphiphilic nanoparticles. Electron and atomic force microscopes and dynamic light scattering techniques confirmed the size and shape of the amphiphilic assembly and its ATP complexes. Isothermal calorimetric experiments were carried out to determine the binding constants for the amphiphilic nanoparticle binding to ATP. The binding of the amphiphilic nanoparticle to ATP was found to be an endothermic process with a binding constant three times higher compared to its precursor Pi. This investigation provides the first insight into the development of a thermo-responsive scaffold for recognition of ATP.

Introduction

The capability of metal salts for 'salting-in' and 'salting-out' proteins[1] or macromolecules[2] from aqueous solution was found to be driven by the anions of the metal salts rather than the cations.[3] This effect is known as the "Hofmeister effect" and the Hofmeister series for the anions is given as:[4] $CO_3^{2-} > SO_4^{2-} > S_2O_3^{2-} > H_2PO_4^- > F^- > Cl^- > Br^- \approx NO_3^- > I^- > ClO_4^- > SCN^-$. The anions at the left end of the series are termed as water "structure makers" (or kosmotropes) and those on the right end of the series are termed as water "structure breakers" (or chaotropes).[5] Theories and experimental methods have been developed to address the mechanism of the Hofmeister effect.[6,7] In macromolecular systems, the influence of anions on thermo-responsive polymers has been found to be of immense importance regarding the fundamental understanding of polymer chain folding and crystallization in the aqueous environment.[8] Poly(*N*-isopropylacrylamide) (PNIPAM)[9,10] and elastin-like polypeptides (ELPs)[11–13] are some of the most extensively studied thermo-responsive commercial polymers for the Hofmeister effect.[8] Wei *et al.* recently reviewed the anticancer drug loading and delivering capabilities of PNIPAM to cancer cells.[14] The Hofmeister effect was also employed to understand enzymatic activity,[15] peptide self-assembly,[16] fluorescent polyacrylates,[17] polyacrylate hydrogels,[18,19] guest–host interactions,[20] cationic polythiophenes,[21] *O*-acylcholines,[22] cationic gemini surfactants[23] and PEO–PPO–PEO triblocks.[24] These studies emphasized the importance of the Hofmeister effect in the self-assemblies of organic materials and polymers. However, no efforts have been made to study the role of the Hofmeister effect in the binding (or sensing) of biologically important anionic species such as adenosine phosphates. It is very important to study the Hofmeister effect of biological phosphate anions since they play significant roles in intra- and extracellular signaling and ion transport.[25] Adenosine triphosphate (ATP) is a multifunctional nucleotide of immense importance in biology as it serves as the molecular currency for intracellular energy generation. Extracellular ATP plays vital roles in several biochemical pathways such as platelet function, neurotransmission, signal transduction, vasodilatation, and muscle contraction.[26] Recent studies have revealed that under physiological conditions, the concentration of extracellular ATP was found to be much higher in cancer tissues compared to normal tissues.[27,28] For extracellular ATP administration studies at tumor sites, the concentrations of ATP typically vary from 1 mM to 5 mM to trigger

Department of Chemistry, Indian Institute of Science Education and Research (IISER), Dr Homi Bhabha Road, Pune 411008, Maharashtra, India. E-mail: jayakannan@iiserpune.ac.in; Fax: +91-20-2590-8187

† Electronic supplementary information (ESI) available: Additional % transmittance plot for AMP, ADP and Pi binding towards the scaffold, DLS data and NMR and MALDI-TOF data. See DOI: 10.1039/c4tb01844c

‡ All authors contributed equally.

apoptosis or programmed cell death.[29,30] The enhancement of the extracellular ATP concentration in cancer tissues is generally promoted by the release of ATP from the cytoplasm mediated *via* several plasma membrane receptors such as ABC transporters, P2X7 receptors, and connexins.[31] Several optical chromophores have been developed to recognize ATP through colorimetric changes[32,33] or fluorescence techniques[34–37] and this topic was recently reviewed by Zhou *et al.*[38] However, the sensing or binding of ATP through the Hofmeister effect by thermo-responsive amphiphiles has not been attempted to date .

The uncontrolled cell division and fast growth make the environment in cancer tissues (42–44 °C; pH = 6.5 to 5.5) very different to normal tissues (37 °C and pH = 7.4).[39] Thermo-chemotherapy is a recently developed drug administration concept to enhance the cytotoxicity of anticancer drugs at least three times by applying temperatures between 40.5 °C and 43.5 °C.[40] Thus, developing thermo-responsive drug carriers that could disassemble either at abnormal tissue temperatures (40–44 °C) or due to external heat stimuli of in thermochemotherapy would enhance the efficacy of the cancer treatment.[41] Additionally, the porous network and defective lymphatic drainage in cancer tissues allow the accumulation of larger size macromolecular or self-assembled polymer particles (150–250 nm) through the enhanced permeability and retention (EPR) effect.[42,43] Existing thermo-responsive materials such as PNIPAM would support the EPR effect; however, they cannot be used for ATP binding since their LCST is lower than 37 °C.[14] Hence, the above multi-task problem could be addressed only by the design of a new thermo-responsive scaffold having "super LCST characteristics" to withstand the Hofmeister effect of anions at cancer tissue temperatures (42–44 °C). In general, ATP binding shows interference with its precursors such as ADP, AMP and Pi (inorganic phosphate); thus, the new scaffold should have preferential selectivity for the detection of ATP among its other anionic precursors. Thus, the new material design requires the following criteria: (i) super LCST characteristics for recognizing ATP through the Hofmeister effect; (ii) it should show selective binding towards ATP over its other precursors in aqueous medium; and (iii) it should have the ability to self-organize into nano-size objects so that it can penetrate through cancer tissues *via* the EPR effect. This concept is schematically shown in Fig. 1.

The present investigation reports one of the first examples of super LCST thermo-responsive amphiphilic nano-scaffolds as a tool to recognize and bind ATP. A new di-block amphiphile was designed with a hydrogen bonded amide linkage that connects both sides, with the hydrophobic unit based on the renewable resource 3-pentadecyl phenol (PDP) and polyethylene glycol chains as the hydrophilic part. PDP was chosen in the present investigation since it was found to be an efficient hydrophobic unit for producing polysaccharide vesicles,[44–46] multi-vesicular bodies[47] and shape transformable thermo-responsive core–shell nanoparticles[48] in our earlier work. Thus, the selection of the hydrophobic PDP unit with the appropriate PEG chain length has facilitated the designing of a thermo-responsive amphiphile that showed the highest LCST > 90 °C (named "super LCST amphiphile"). This thermo-responsive scaffold followed the typical Hofmeister series and exhibited preferential binding towards ATP at 42–44 °C. Dynamic light scattering, electron and atomic force microscopes provided direct evidence for the mechanism of nanoparticle driven ATP detection. Further, isothermal calorimetric experiments were also carried out to

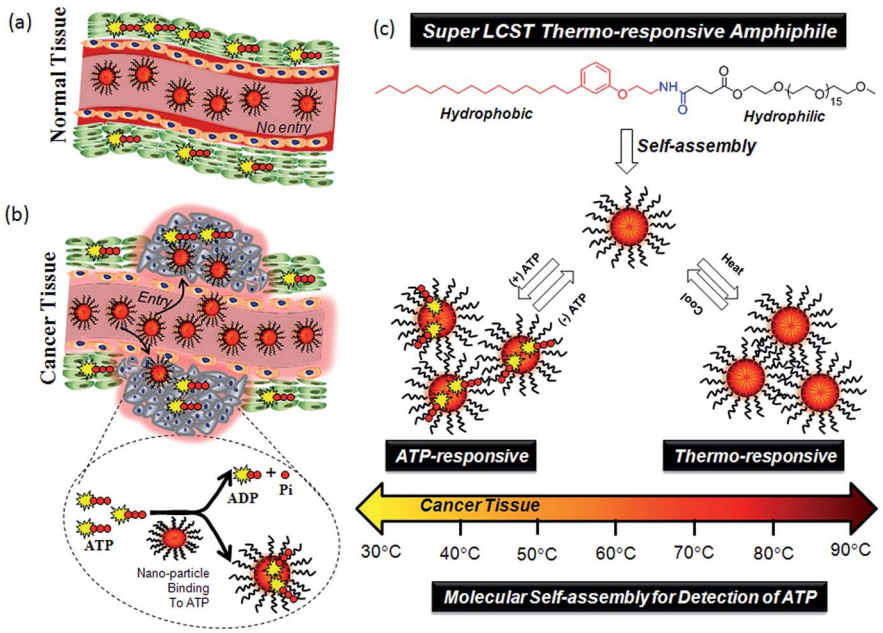

Fig. 1 Thermo-responsive amphiphilic nanoparticle entry in normal tissue (a) and cancer tissue (b) environments. The expanded part in b demonstrates the ATP pathways for hydrolysis and binding to the nanoparticle. (c) A di-block molecular design for the super LCST amphiphile **1** and the self-assembly of the amphiphilic nanoparticle towards ATP.

determine the association constants for the selective binding of the thermo-responsive nanoparticle to ATP.

Experimental methods

Materials

3-Pentadecylphenol, 2-ethanolamine, succinicanhydride, Boc-anhydride triethylamine (Et_3N), polyethylene glycol monomethylether (MW = 750), 1-ethyl-3-(3-dimethylaminopropyl) carbodiimide (EDC), diisopropyl ethylamine (DIPEA), and diisopropyl azodicarboxylate (DIAD) were purchased from Aldrich chemicals. All other reagents and solvents were purchased locally and purified following standard procedures. The *tert*-butyl (2-hydroxyethyl) carbamate was synthesized using our earlier report.[44]

General procedures

^{1}H-NMR and ^{13}C-NMR spectra were recorded using a 400 MHz Jeol NMR spectrophotometer in $CDCl_3$ containing TMS as the internal standard. Infra-red spectra were recorded using a Thermo-Scientific Nicolet 6700FT-IR spectrometer with the solid state in KBr. The masses of the amphiphiles and all the intermediates were confirmed using the Applied Biosystems 4800 PLUS MALDI TOF/TOF analyzer. The purity of the amphiphile was determined by gel permeation chromatography (GPC) using a Viscotek VE 1122 pump, Viscotek VE 3580 RI detector, and Viscotek VE 3210 UV/Vis detector in tetrahydrofuran (THF) using polystyrene as the standard. The optical transmittance measurement was done using a PerkinElmer Lambda 45 UV-Visible spectrophotometer. The size determination of the aqueous solution of the amphiphile was carried out by dynamic light scattering (DLS) using a Nano ZS-90 apparatus utilizing a 633 nm red laser (at 90° angle) from Malvern instruments. The reproducibility of the data was checked for at least three independent solutions. FE-SEM images were recorded using a Zeiss Ultra Plus scanning electron microscope. For FE-SEM analysis, the samples were prepared by drop casting on silicon wafers and then coating with gold. TEM images were recorded using a Technai-300 instrument by drop casting the sample on a Formvar-coated copper grid. The ITC measurement was carried at 25 °C using an iTC200 microcalorimeter (MicroCal Inc.). Atomic force microscope images were recorded for drop cast samples using JPK instruments attached with Nano wizard-II setup.

Optical transmittance measurement

The optical transmittance of PDP-PEG750 was measured at 500 nm using a quartz cell (path length: 1 cm) with a PerkinElmer Lambda 45 UV-Visible spectrophotometer equipped with a temperature-controller. The heating cycle was recorded by heating the sample continuously from 30 °C to 90 °C. Similarly, the cooling cycle was recorded from 90 °C to 30 °C. The heating and cooling cycles were maintained at a rate of 10° min^{-1} using a Peltier heating/cooling source.

Isothermal titration calorimetry (ITC)

The titrations of ATP and the inorganic phosphate anion with the scaffold (PDP-PEG-750) were performed at 25 °C using an iTC200 microcalorimeter (MicroCal Inc.). In these experiments, ATP and the inorganic phosphate anion were titrated into a scaffold solution. Both the solution in the injection syringe and the one in the ITC cell were prepared in water. Two blank titrations were also performed: (i) titration of water with the same ATP and Pi solution; and (ii) titration of the amphiphile with water. The stoichiometries of substrate binding (n) and the binding constants (K_a) of amphiphile **1** with ATP and Pi were obtained after subtracting the blank titrations. The stirring speed used was 1000 rpm and the reference power was set at 0.5 μcal s^{-1} for all the titrations. The volume of the ITC200 cell was 0.200 mL while that of syringe was 0.040 mL.

Cell viability assay (MTT assay)

To test the cytotoxicity of the amphiphile **1**, a cell viability assay was performed in HeLa cell lines using the tetrazolium salt 3-(4,5-dimethylthiazol)-2,5-diphenyl tetrazolium bromide (MTT). HeLa cell lines (1×10^3) were seeded in each well in a 96 well plate (Corning, USA) in 100 μL of DMEM with 10% FBS (fetal bovine serum) and allowed to adhere for 12 h and 24 h. Prior to drug treatment, the medium from the cells was aspirated and various concentration of amphiphile **1** were prepared. These were added to 100 μL of DMEM with FBS in which the cells were incubated. Blank controls, DMEM with FBS in the absence of cells, were used in each experiment. All control and treated experiment wells were done in triplicate. Cells were incubated for 12 h and 24 h without a change in medium, and after 12 h and 24 h, the amphiphile **1** medium was aspirated. Freshly prepared stock of MTT in sterile PBS (5 mg mL^{-1}) was diluted to 50 μg mL^{-1} in 100 μL of DMEM with FBS and was added to the cells. The cells were then incubated with MTT for 4 h at 37 °C. The medium with MTT was then aspirated from the wells and the purple formazan crystals formed as a result of the reduction of MTT by mitochondrial dehydrogenase enzyme from the cells dissolved in 100 μL of 100% N,N-dimethylsulfoxide (DMSO) (added per well). The absorbance from the formazan crystals was immediately measured using a microplate reader at 570 nm (Varioskan Flash) and is representative of the number of viable cells per well. Values from the triplicates for each control and treated set were noted and their means used for calculations. The mean of the absorbance values for the blank control samples was subtracted from the average of the treated samples. The values thus obtained for the control samples were equated to 100% and relative percentage values for amphiphile **1** were calculated accordingly.

Synthesis of PEG750-COOH (PEG-Acid)

Poly(ethylene glycol) MW 750 monomethylether (10.0 g, 13.0 mmol) and succinic anhydride (1.6 g, 16.0 mmol) were dissolved in dry dichloromethane (60 mL) and purged under N_2 for 10 min. To this reaction mixture, Et_3N (1.85 mL, 13.0 mmol) was added drop wise. Immediately after the addition of Et_3N the

reaction mixture started to boil vigorously. The reaction proceeded at 25 °C for 48 h with continuous stirring under N_2 atmosphere. The reaction mixture was poured into water (100 mL) and was neutralized with 2 N concentrated HCl (2.0 mL). The organic layer was washed with brine solution, dried over anhydrous sodium sulfate and concentrated to obtain a yellow liquid as the product. It was purified by passing through a silica gel column of 60–120 mesh using 50% methanol in chloroform as the eluent. Yield = 6.0 g (66%). ^{1}H NMR ($CDCl_3$, 400 MHz) δ: 4.14 ppm (t, 2H, CO–OCH_2), 3.56–3.50 ppm (s, 66H, OCH_2–CH_2O), 3.23 ppm (s, 3H, CH_2–OCH_3), 2.52 ppm (s, 4H, CO–CH_2–CH_2). ^{13}C NMR ($CDCl_3$, 100 MHz) δ: 177.05 (*C*OOH), 171.88 (*C*OO–CH_2), 70.56 (OCH_2–*C*H_2–O), 69.93 (COO–*C*H_2), 58.51 (C–OCH_3), 28.45 (CO–*C*H_2–*C*H_2). FT-IR (cm^{-1}): 3448, 2875, 1727, 1649, 1453, 1349, 1286, 1247, 1202, 1087, 947, 842, 677, 622. MALDI-TOF-MS: *m*/*z* calculated for $C_{39}H_{76}O_{21}$: 880 and found: 903 ($M^+ + Na^+$).

Synthesis of *tert*-butyl-2-(3-pentadecylphenoxy)ethyl carbamate (PDP-NH-Boc)

tert-Butyl(2-hydroxyethyl) carbamate (3.7 g, 23.0 mmol), 3-pentadecylphenol (7.0 g, 23.0 mmol) and triphenylphosphine (6.6 g, 25.0 mmol) were dissolved in dry tetrahydrofuran (20 mL). The contents were then placed in an ice-cooled bath for 10 min with continuous N_2 purge. To this ice-cooled reaction mixture, diisopropyl azodicarboxylate (4.47 mL, 23.0 mmol) was added drop wise under N_2 atmosphere. The reaction mixture was further stirred at 25 °C for 24 h. It was purified by passing through a silica gel column of 60–120 mesh using 1% ethyl acetate in hexane as the eluent. Yield = 8.0 g (66%). ^{1}H NMR ($CDCl_3$, 400 MHz) δ: 7.19 ppm (t, 1H, Ar–*H*), 6.80–6.70 ppm (m, 3H, Ar–*H*), 5.02 ppm (s, 1H, N*H*), 4.02 ppm (t, 2H, Ar–OCH_2), 3.54 ppm (t, 2H, CH_2–N), 2.58 ppm (t, 2H, Ar–CH_2), 1.46 ppm (s, 9H, OC–C(CH_3))$_3$, 1.6–0.88 ppm (m, 29H, aliphatic H). ^{13}C NMR ($CDCl_3$, 100 MHz) δ: 158.62 (Ar–C), 155.98 (*C*O–O), 144.85, 129.29, 121.32, 114.75, 111.40 (Ar–C), 79.57 (O*C*(CH$_3$))$_3$, 67.08 (Ar–OCH_2), 40.26 (CH_2–N), 36.09, 32.00, 29.76, 26.47, 22.77, 14.20. FT-IR (cm^{-1}): 3396, 2916, 2850, 1690, 1590, 1512, 1453, 1362, 1250, 1157, 1060, 95, 866, 778, 690. MALDI-TOF-MS: *m*/*z* calculated for $C_{28}H_{49}NO_3$: 447 and found: 470 ($M^+ + Na^+$).

Synthesis of 2-(2-(2-methoxyethoxy)ethoxy)ethyl 4-oxo-4-((2-(3-pentadecylphenoxy)ethyl)amino)butanoate (amphiphile 1)

PDP-NH-Boc (2.0 g, 44.0 mmol) was dissolved in dichloromethane (5.0 mL) and to this mixture trifluoroacetic acid (10.0 mL, 129.7 mmol) was added drop wise. The contents were stirred at 25 °C for 1 h and then the solvent was evaporated by Rotavapor. The TFA was removed by adding fresh DCM (10.0 mL × 3 times) and was evaporated by Rotavapor. The content was further poured into ice-cooled diethyl ether (15.0 mL) and evaporated by Rotavapor to obtain a white solid as the product. The white solid product (1.34 g, 3.8 mmol) was dissolved in dry dichloromethane (20.0 mL) and was purged with N_2 for 15 minutes. To it, PEG-Acid (3.0 g, 3.5 mmol) was added and N_2 purging was continued for the next 15 minutes. To this reaction mixture, EDC (0.81 g, 4.2 mmol) and diisopropylethylamine (1.4 mL, 7.8 mmol) were added under N_2 atmosphere and the reaction was then left at 25 °C for 48 h with continuous stirring. It was then poured into water (30.0 mL) and the product was extracted into chloroform. The organic layer was washed with 10% $NaHCO_3$ (30.0 mL), neutralized with 2 N HCl (6.0 mL), dried over anhydrous sodium sulfate and concentrated to obtain a yellow liquid as the product. It was further purified by passing through a silica gel column of 60–120 mesh using 5% methanol in chloroform as the eluent. Yield = 2.27 g (54.0%). ^{1}H NMR ($CDCl_3$, 400 MHz) δ: 7.18 ppm (t, 1H, Ar–*H*), 6.80–6.70 ppm (m, 3H, Ar–*H*), 6.24 (CO–N*H*), 4.24 ppm (t, 2H, COO–CH_2), 4.02 ppm (t, 2H, Ar–OCH_2), 3.69–3.66 ppm (m, 75H, O–CH_2–CH_2), 3.56 ppm (t, 2H, CH_2–N), 3.38 ppm (s, 3H, CH_2–OCH_3), 2.70 ppm (t, 2H, Ar–CH_2), 2.57 ppm (t, 2H, NH–CO–CH_2), 2.51 ppm (t, 2H, CH_2–COO), 1.6–0.88 ppm (m, 29H, aliphatic H). ^{13}C NMR ($CDCl_3$, 100 MHz) δ: 172.87 (NH–*C*O), 171.60 (*C*O–O), 158.54, 144.86, 129.32, 121.36, 114.69, 111.47 (Ar–C), 72.00 (*C*H_2–OCH_3), 70.64 (O–*C*H_2–*C*H_2), 69.07, 66.65 (Ar–OCH_2), 63.83 (COO–*C*H_2), 59.11 (O–CH_3), 39.16 (CH_2–N), 36.09, 31.99, 31.49, 29.75, 29.43, 22.76, 14.19. FT-IR (cm^{-1}): 3374, 2916, 2878, 1735, 1651, 1599, 1551, 1460, 1347, 1278, 1244, 1103, 955, 846, 784, 751, 697. MALDI-TOF-MS: *m*/*z* calculated for $C_{62}H_{115}NO_{21}$: 1121 and found: 1144 ($M^+ + Na^+$).

Results and discussion

Synthesis and thermo-responsiveness of amphiphile 1

An amphiphilic molecule was synthesized from polyethylene glycol monomethyl ether MW = 750 g mol^{-1} as the hydrophilic part and the renewable resource pentadecyl phenol (PDP) as the hydrophobic unit, as shown in Scheme 1. Succinic anhydride was ring opened with PEG in the presence of Et_3N, which acts as a base to give PEG-Acid. *tert*-Butyl (2-hydroxyethyl) carbamate was coupled with PDP in the presence of diisopropyl azodicarboxylate and triphenylphosphine to give *tert*-butyl (2-(3-pentadecy-8-en-1-yl) phenoxy) ethyl carbamate (PDP-NH-Boc). The carbamate was then treated with trifluoroacetic acid (TFA) to give 2-(3-pentadecy-8-en-1-yl) phenoxy ethanamine, which was further coupled with PEG-Acid in the presence of EDC and diisopropylethyl amine (DIPEA) to give amphiphile **1**.

The structure of amphiphile **1** was characterized by ^{1}H and ^{13}C-NMR (see ESI SS-1†). The MALDI-TOF spectrum of amphiphile **1** showed the distribution of mass peaks in the range of the range of *m*/*z* 900 to 1500 (see Fig. 2(a)). The mass differences between the adjacent peaks were obtained as 44 amu with respect to the distribution in the PEG chains in the diblock amphiphile **1**. The mass of each peak was calculated using the formula: (44.05)*n* + 461 + 23, where 44.05 is the repeating unit mass of PEG units and 461 and 23 correspond to the mass of the hydrophobic unit and the sodium ion, respectively. The mass of the peak corresponding to $n = 15$ is shown by an arrow. The thermo-responsive behavior of amphiphile **1** was studied by optical transmittance measurement as a function of temperature using an absorbance spectrophotometer. The plots of optical transmittance in the heating and cooling cycles are shown in Fig. 2(b). The plots reveal that the transmittance of the aqueous solution of amphiphile **1** decreases from 97% to 10%

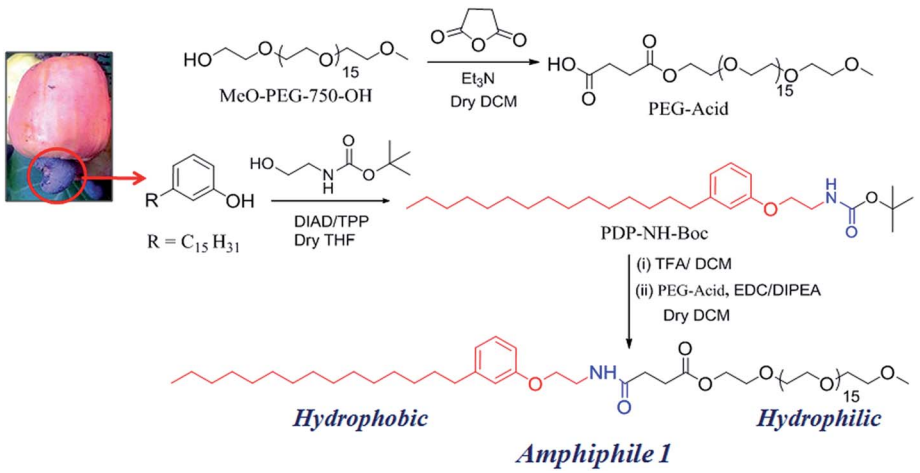

Scheme 1 Synthesis of the thermo-responsive amphiphile **1**.

at 92 °C (LCST). From the plots it is also evident that both the heating and cooling cycle follow the same kinetic path, indicating that changes in the aggregates with temperature occur at similar rates. In other words, the assembly and disassembly of the aggregates do not exhibit hysteresis.

The temperature-driven self-assembly was further studied by subjecting the aqueous solution of amphiphile **1** (10^{-4} M) to variable temperature dynamic light scattering (DLS). The DLS histograms recorded for amphiphile **1** in the heating and cooling cycles are shown in Fig. 2(c) and (d), respectively. Amphiphile **1** showed a mono-modal distribution indicating the formation of uniform size aggregates in water. Further, it showed a sharp increase in the hydrodynamic diameter from 140 ± 30 nm (below the LCST) to 600 ± 30 nm with respect to the formation of larger aggregates above the LCST. The reversibility of the thermo-responsive self-assembly process was further inferred from the cooling cycle (see Fig. 2(d)). It is important to mention that the DLS histograms are broad at low temperature; however, they become very narrow while approaching the LCST temperature (see Fig. 2(c)). On the other hand, in the subsequent cooling cycle (see Fig. 2(d)), the DLS histograms also retained the narrow distribution at room temperature. The reversibility of the amphiphilic self-assembly was further confirmed by repetitive scanning in the continuous heating and cooling cycles (see Fig. SF-1†). The size of the aggregates varied from 140 ± 20 nm to 600 ± 35 nm with perfect reproducibility. This implies that the temperature induced self-assembly process in amphiphile **1** is completely reversible;

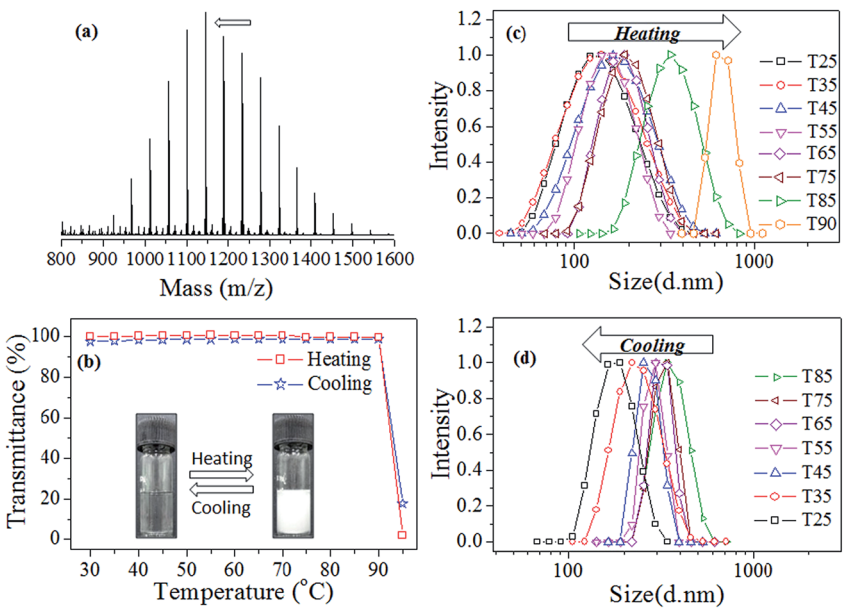

Fig. 2 (a) MALDI-TOF spectrum of amphiphile **1** and the repeating unit mass for the peak at $n = 15$ is shown by arrow. (b) Temperature dependent optical transmittance of amphiphile **1** in water in consecutive heating and cooling cycles. DLS histogram of amphiphile **1** in the heating (c) and cooling (d) cycles. The concentration of amphiphile **1** is 10^{-4} M.

however, the dis-assembly occurred more uniformly as compared to the self-assembling process in the cooling and heating cycles, respectively.

To visualize the size and shape of the nano-aggregates, amphiphile **1** was subjected to field emission-scanning electron microscopy (FE-SEM), high resolution transmission electron microscopy (HR-TEM) and atomic force microscopy (AFM) analysis. In Fig. 3(a), the FE-SEM image of amphiphile **1** showed the formation of spherical shape particles of 170 ± 22 nm diameter. The HR-TEM image of these particles confirmed that these spherical aggregates (150 ± 20 nm in size) are hard spheres with respect to micellar nanoparticles (see Fig. 3(b)). The AFM image of amphiphile **1** also confirmed the existence of spherical nanoparticles of 130 ± 25 nm (see Fig. 3(c)). The HR-TEM image of the nano-aggregates above the LCST is shown in Fig. 3(d). Above the LCST, the nanoparticles of size 140 ± 20 nm were found to form clusters together as larger aggregates. The sizes of the nano-particulate assemblies below and above the LCST from the microscope images matched very well with their solution aggregates in DLS (see Fig. 2(c) and (d)). The critical micellar concentration (CMC) of the amphiphile was determined using Nile red as a fluorescent probe. Nile red is a hydrophobic dye that is insoluble in water and displays no fluorescence in aqueous medium. Once it has been sequestrated in the hydrophobic core, the fluorescence is generated and can be used as an indicator of the formation of the micellar aggregates (see SF-2†). The concentration of Nile red was kept constant (0.2 μM) while the concentration of amphiphile **1** was varied from 1.0 μM from 1.0 mM (see SF-2†). The emission intensity of the Nile red was plotted against the concentration (see SF-2†) . The plot showed break point at 1.0×10^{-5} M with respect to its CMC. The Nile red encapsulation study also suggests that the thermo-responsive micellar assemblies could be useful for loading diverse hydrophobic molecules in their inner core, including anticancer drug molecules.

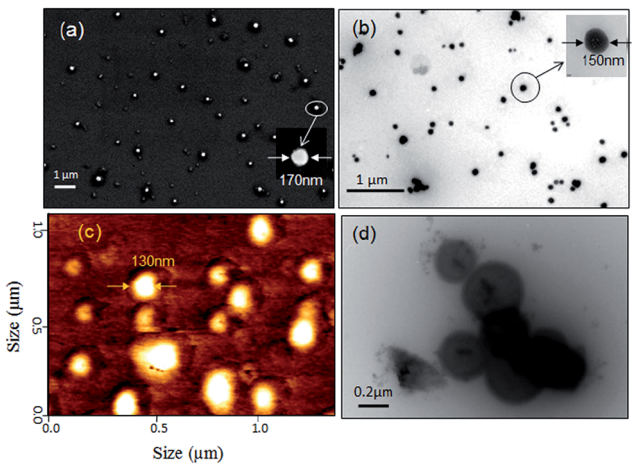

Fig. 3 (a) FE-SEM image, (b) HR-TEM image and (c) AFM image of amphiphile **1** below the LCST (25 °C). (d) HR-TEM of amphiphile **1** above the LCST at 90 °C. The concentration of amphiphile **1** is 10^{-4} M for the imaging.

Hofmeister effect of amphiphile 1

Three anion sources were chosen to investigate the Hofmeister effect on the LCST of amphiphile **1**: NaSCN, a strong chaotrope (water "structure breaker"), NaCl and Na_2SO_4, a strong kosmotrope (water "structure maker"). The plot of transmittance (%) as a function of temperature at various concentrations of Na_2SO_4 is shown in Fig. 4(a) (for NaCl and NaSCN, see SF-3 and SF-4†). The transitions appeared in two phases and this behavior is attributed to: (i) the initial fast binding of the anions to the nanoparticles; (ii) followed by the diffusion controlled slow binding process due to the precipitation of the amphiphile. At the initial stage, the homogeneous environment facilitates the fast binding whereas the heterogeneous precipitation at the secondary stage became a diffusion process. The onset of the cloud point in the heating cycle is termed as the turbidity 'turn-on temperature' while the temperature at which turbidity gets cleared completely is termed as the 'turn-off temperature'. The 'turn-on temperatures' for Na_2SO_4, NaCl and NaSCN (see Fig. 4(b)) revealed that the SO_4^{2-} anion showed higher salting out compared to Cl^- ions while the SCN^- ions did not induce any change in the LCST of the amphiphile. At very high concentrations (above 500 mM), a large amount of precipitation occurred and the error became very high. This is one of the main reasons that the Hofmeister effect could not be studied for more than 600 mM salt concentration. The lowering of the LCST from 90 °C to 55 °C in the presence of the sulfate ion was attributed to the binding of anions towards the amide and PEG-chains, which altered the hydration shell in the micellar assemblies. The reduction in the hydration induces the precipitation of the PEG chains on the periphery of the nano-particulate assemblies which results in the turbidity. During precipitation, many nanoparticles come together as a result of nucleation followed by growth. This process is evident from the DLS and HR-TEM images, as shown in Fig. 3. This experiment confirmed that the newly designed thermo-responsive amphiphile **1** showed binding towards anions and follows the Hofmeister series.

To further validate the Hofmeister effect of the present molecular design, another thermo-responsive diblock with triethylene glycol (TEG) as the hydrophilic unit (in the place of PEG chains) was chosen and subjected to the anion studies (see the structure PDP-TEG in SF-5†). This short amphiphile has a LCST of 42 °C, which is much lower compared to the LCST of amphiphile **1** (90 °C) (see SF-5†). This indicates that the super LCST nature of the amphiphile arose from the long PEGylated chains in the diblocks design strategy (see Scheme 1). Surprisingly, the short amphiphile PDP-TEG lost its LCST behaviors upon binding to the anions. This clearly supports the structure of the thermo-responsive material being very crucial for studying the Hofmeister effect towards anions. In the present case, the super LCST amphiphile **1** provided an appropriate hydrophilic and hydrophobic balance for the above purpose. Recently, Cremer and co-workers reported that the LCST of the PNIPAM and elastic-like peptide decreased upon complexation with the anions by 10–11 °C in the presence of the SO_4^{2-} anion.[9] In the present case, the LCST of amphiphile **1** decreased by

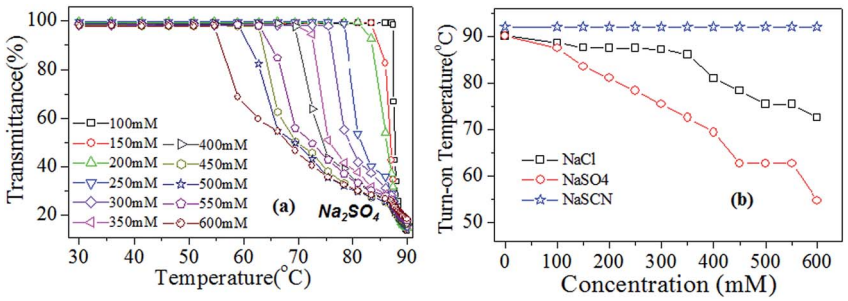

Fig. 4 (a) Temperature dependent transmittance of amphiphile **1** with various concentrations of Na_2SO_4. (b) Turn-on temperature at various concentrations of NaSCN, NaCl and Na_2SO_4.

35 °C upon binding to the SO_4^{2-} anion. It suggests that amphiphile **1** experienced the Hofmeister effect as equivalent to that of the high molecular weight thermo-responsive PNIPAM. Thus, amphiphile **1** has an appropriate molecular design with super LCST characteristics for binding or sensing anions in a large temperature window from 90 °C to 30 °C.

ATP binding

Biological anions such as adenosine triphosphate (ATP) and its precursors ADP (adenosine diphosphate), AMP (adenosine monophosphate) and inorganic phosphate (Pi) were chosen to test the binding abilities of the thermo-responsive nano-scaffold. Under physiological conditions, ATP ecto-nucleotidase hydrolyzes ATP into ADP and Pi with the release of 30.5 kJ mol^{-1} of energy, which is further utilized for several biological processes (see Fig. 5(a)). The amphiphile **1** was subjected to optical transmittance measurement with variable concentrations of nucleotides and their % transmittance in the heating and cooling cycles are shown in Fig. 5(b) and (c), respectively (for Pi, ADP, and AMP SF-6, SF-7 and SF-8†). From the heating cycle (see Fig. 5(b)), it is evident that with an increase in concentration of ATP, the LCST of the nano-particulate assembly significantly reduced. This is attributed to the tendency of ATP to alter the hydration shell at the periphery of the nanoparticle, which results in the precipitation of PEG chains (as similar to SO_4^{2-} ions). In the subsequent cooling cycle (see Fig. 5(c)), the amphiphile + ATP complex showed a slow disassembly process and the complex was stable up to 42–44 °C at the higher concentration of ATP. The non-reversibility of the ATP aggregates sizes in the cooling cycles was checked in repeat experiments (SF-9†). The reason for this stable assembly is not clear at present; however, it implies that the large accumulation of ATP in cancer tissues could preserve the amphiphile **1** + ATP complex in a stable form. The ATP binding studies were further subjected to variable temperature dynamic light scattering (DLS) measurements for fixed concentrations of ATP (300 mM) and scaffold (see Fig. 5(d) and (e)). The hydrodynamic diameter from the heating and cooling cycle was plotted against temperature and is shown in Fig. 5(f). From the heating cycle, it is evident that the size of the aggregates increased gradually from 300 nm to 1.7 μm with the increase in temperature. On the other hand, in the cooling cycle the size of the aggregates did not change much and retained the size in the micrometer range. This indicates that the complex formation between ATP and the nanoparticle produced larger size aggregates in the heating cycle; however, they did not di-assemble into the individual nanoparticle and ATP in the subsequent cooling. This implies that once the nanoparticles bind to ATP, they would not disassociate or release the ATP molecule immediately (see Fig. 1(b)). It is also important to note that the scaffold alone did not show any larger change in size in the heating/cooling cycles (see Fig. 2(c) and (d)); thus, the non-occurrence of disassembly observed in Fig. 5(d)–(f) corresponds to the formation of a stable ATP + scaffold.

Further, the aggregation phenomenon of the nanoparticle in the presence of ATP was validated by subjecting the scaffold + ATP complex to HR-TEM analysis. The HR-TEM images of the nano-aggregates showed the scaffold + ATP complex as individual nanoparticles below the LCST (see Fig. 5(g)). Above the LCST, the nanoparticles were assembled together to produce micrometer sized aggregates (see Fig. 5(h)). This morphological assembly was further evident from the observation in the % transmittance and DLS (see Fig. 5(d) and (e)). The photographs of vials containing the scaffold with ATP, ADP, AMP and Pi at 45 °C are shown in Fig. 5(i). Only the ATP + scaffold complex showed turbidity at 45 °C indicating that the nanoparticle assembly has preferential binding towards ATP compared to other nucleotides. This is further supported by variable temperature DLS analysis of the scaffold in the presence of Pi (see SF-10†). The size of the aggregates increases from 250 nm to 750 nm upon heating (see SF-11†) while in the cooling cycle (see SF-11†) it completely reverts to its original size. This suggests that the complex formed between the scaffold and Pi is not stable, unlike its ATP complex. ADP and AMP did not show any remarkable changes in the LCST of the nanoparticle (see SF-7 and SF-8†). These control experiments confirmed that the thermoresponsive nanoparticle has preferential binding towards ATP.

In order to shed more light on the selectivity of amphiphile **1** towards ATP, the differences in the turn-on and turn-off turbidity temperatures of the scaffold in the presence of ATP, ADP, AMP and Pi were plotted and are shown in Fig. 6(a) and (b). The plot of turn-on temperature as a function of concentration reveals that the affinity of amphiphile **1** was significantly more towards ATP as compared to ADP, AMP and Pi. The 'turn-

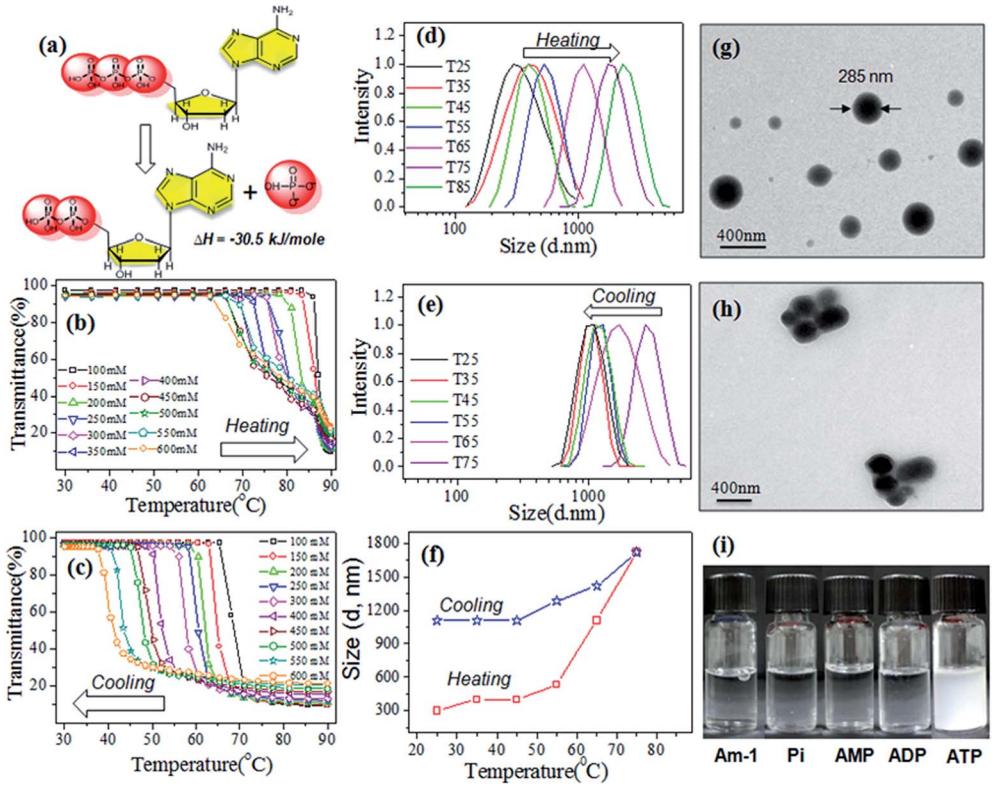

Fig. 5 (a) Mechanism of ATP hydrolysis into ADP and inorganic phosphate (Pi). Temperature dependent optical transmittance of amphiphile **1** in water at various concentrations of ATP in the heating (b) and (c) cooling cycles. Temperature dependent DLS histogram of amphiphile **1** in water in presence of adenosine triphosphate (ATP) (300 mM) in the heating cycle (d) and cooling cycle (e). (f) Plot of hydrodynamic diameter against temperature in the heating and cooling cycles. HR-TEM image of the ATP–amphiphile **1** complex in water below the LCST (g) and above the LCST (h). (i) Photograph of amphiphile **1** with ATP AMP, ADP and Pi in water at 45 °C. The concentration of amphiphile **1** is 10^{-4} M and the concentrations of the analytes are 300 mM.

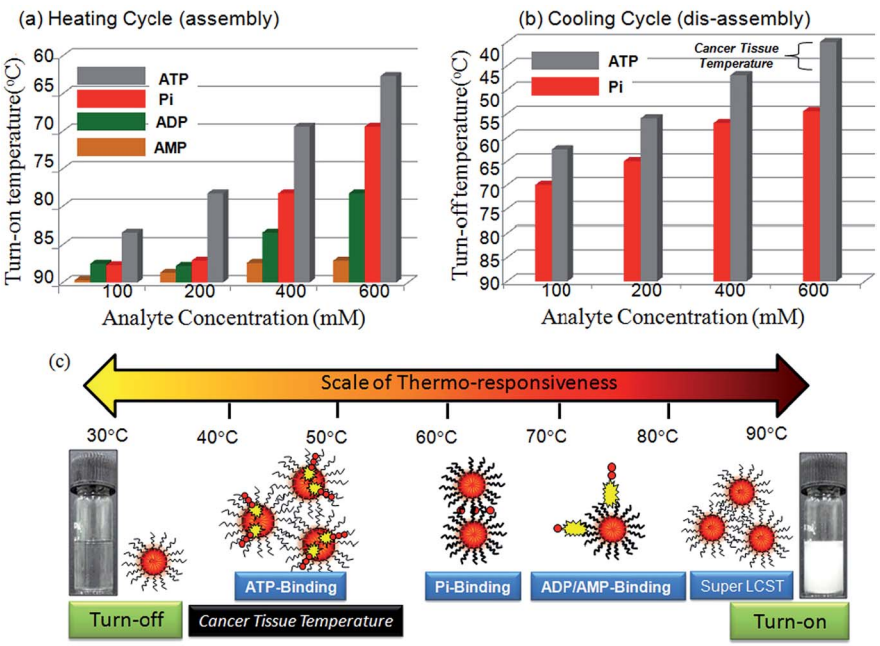

Fig. 6 (a) Plot of turn-on temperature of amphiphile **1** as a function of concentration of ATP, ADP, AMP and Pi. (b) Plot of turn-off temperature of amphiphile **1** as a function of concentration of ATP and Pi. (c) Temperature-sensing scale of amphiphile **1** for the ATP, ADP, AMP and Pi.

off temperature' plot revealed that ATP could bring down the scaffold LCST to 45 °C. On the other hand, in the case of Pi it only reaches 70 °C. This suggests that the nanoparticle is efficient to bind ATP over its precursors. The reason for the efficient binding of ATP towards the amphiphile was attributed to the occupation of ATP in the micellar scaffold. ATP has three phosphate anionic groups that are hydrophilic and well separated from the hydrophobic adenosine + sugar units (see Fig. 5(a)). Recently, Wang *et al.*[49] and Liu *et al.*[50] independently reported that the ATP anion binding to the polymer nanoparticle or liposomes were found to be driven by host and guest interactions through the hydrophobic inner core of the nanoassemblies. Further, it was found that ADP and AMP were found to lack perfect guest geometry to occupy the hydrophobic host pocket.[48] Thus, in the present case, during the complexation with the amphiphile, the hydrophobic part of ATP could penetrate into the hydrophobic core of the micellar nanoparticle through like–like interactions. These geometrical arrangements provide better contact between the ATP hydrophilic phosphate groups towards the amide and PEG chains in the micellar exterior shell (see Fig. 6(c)). This arrangement gives the ATP aromatic core in the hydrophobic pocket of the nanoparticle and the anion projecting towards the amide and PEG chains to maximize the Hofmeister effect. As a result, the ATP anion induced maximum influence on the hydration of the amphiphilic scaffold through the Hofmeister effect that reduces the LCST of the ATP + scaffold complex. However, in the case of inorganic Pi, the inorganic anion could easily diffuse as compared to AMP and ADP in the hydroshell of the PEGylated chains at the nanoparticle exterior to significantly induce the Hofmeister effect. Further, to estimate the dynamic range of the ATP binding, the concentration of amphiphile was fixed at 10^{-4} M and the ATP concentration was varied from 10 mM to 100 mM (see SF-12†). The plots showed that the change in the LCST phenomena could be detected in transmittance mode at minimum [ATP] = 100 mM.

This mechanism is further supported by the large increase in the size of amphiphilic scaffold in the ATP + scaffold complex as compared to that of nascent scaffold. For example, the sizes of the scaffold doubled from 140 nm to 300 nm upon binding to ATP at 25 °C (see Fig. 2(c) and 5(d) for 25 °C). This large increase in the size of the scaffold is attributed to the encapsulation of ATP in the micellar core of the amphiphilic self-assembly. On the other hand, both ADP and AMP have an inadequate hydrophilic and hydrophobic balance. Thus, the shape specific encapsulation towards the micellar nanoparticle is not effective to show the Hofmeister effect. Inorganic phosphates affect the scaffold like any other kosmotropes (like sulfate anions) and this was supported by no change in the size of the micellar assemblies after binding to Pi (see SF-11†). Hence, the ATP complexation towards the nanoparticle assembly is the natural choice for maximizing the Hofmeister effect though host–guest interactions. The temperature ranges at which ATP, ADP, AMP and Pi are active on the amphiphilic scaffold are shown in the scale with their possible self-assembled structures in Fig. 6(c). The cytotoxicity of the super LCST amphiphile **1** towards the cancer tissue was checked in HeLa cell lines at 37 °C using the MTT assay. The cells were treated for 12 h and 24 h and the data are shown in Fig. 7. The cells showed more than 85% cell viability below 1 μg mL^{-1}. At higher amphiphile concentrations (5 μg mL^{-1} and 10 μg mL^{-1}), the cells showed 75% viability. For most drug delivery research, the polymer or scaffold concentrations used are typically <1.0 μg mL^{-1}; thus, the new renewable resource based LCST amphiphile may be a very useful biomaterial.

Isothermal calorimetry and binding constants

Isothermal titration calorimetry (ITC) directly measures the heat of the complexation (enthalpy, ΔH), the stoichiometry of substrate binding (n), and the binding constant (K_a). The binding efficiency of ATP and its close interfering anion Pi (based on Fig. 6(b)) with the scaffold were further evaluated by ITC and the data are provided in Fig. 8. The titration of ATP with the nanoparticle displayed endothermic curves (see Fig. 8(a)) while exothermic curves were obtained for titration of the phosphate anion (see Fig. 8(b)). Further, the binding constant for the ATP and phosphate anion complexes with the nanoparticle were found to be 2230 M^{-1} and 719 M^{-1}, respectively. The three times higher binding constant for the ATP towards the scaffold indicates that the ATP binding was stronger than the inorganic phosphate anion.

Earlier ITC reports for ATP binding to poly(dC) (double stranded DNA made up of cytosine)[51] and 3-phophoglycerate kinase[52] showed binding constants of 2.45×10^4 M^{-1} and 3.5×10^{-3} M^{-1}, respectively. The binding constant of the ATP-nanoparticle complex in the present case has a value similar to the above examples. Hence, it can be said that the affinity of the thermo-responsive nanoparticles towards ATP was very good as similar to that of DNA and proteins. Further, the ATP binding to the amphiphilic scaffold is endothermic; thus it was a natural choice for thermodynamically binding in the high temperature environment of the cancer tissue compared to normal tissues. Additionally, the amphiphilic nanoparticle has encapsulation capabilities for hydrophobic dyes and this concept may be expanded to load and deliver water insoluble anticancer drugs. This may provide the additional advantages of simultaneous binding of ATP and releasing the drugs at the cancer tissue temperature. Based on the above studies, it may be summarized

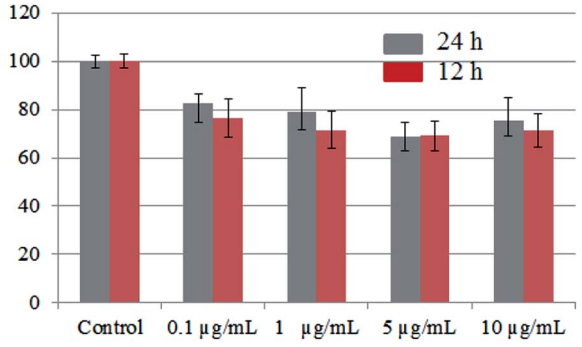

Fig. 7 Cytotoxicity data of amphiphile **1** at various concentrations in MTT assay at 24 h and 12 h.

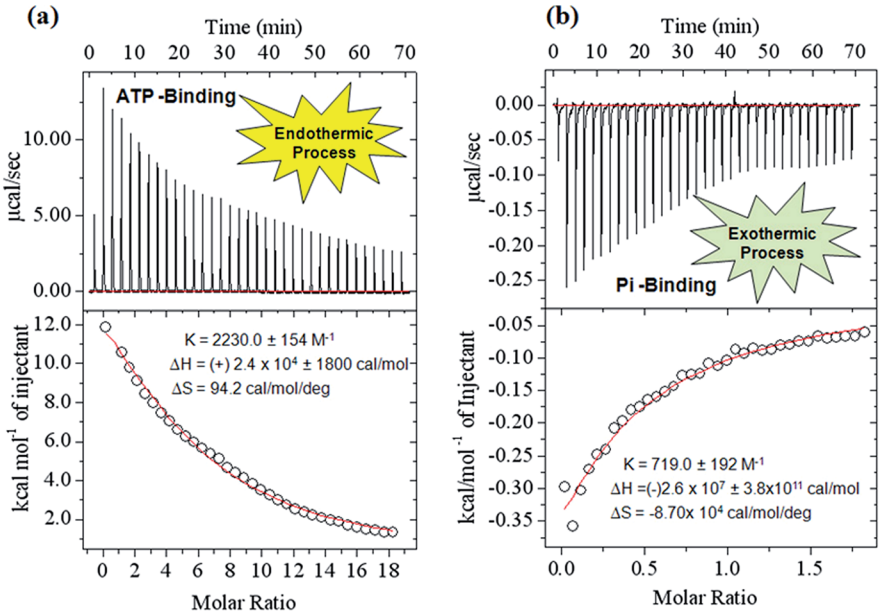

Fig. 8 (a) Isothermal calorimetric titration curves for the binding of amphiphile **1** (0.1 mM) with ATP (10 mM) at 25 °C. (b) Calorimetric curves for the binding of amphiphile **1** (1 mM) with Pi (10 mM) at 25 °C.

that the newly developed thermo-responsive amphiphilic nanoparticle could be useful for targeting ATP as a trigger and also as a carrier for drugs to cancer tissues.

Conclusion

In conclusion, a new thermo-responsive molecular assembly was developed to detect and bind to ATP in aqueous medium. The amphiphilic molecule was designed with an appropriate hydrophilic polyethylene glycol (PEG 750) unit and the renewable resource 3-pentadecylphenol hydrophobic to produce the super LCST amphiphile with an LCST of more than 90 °C in water. Amphiphile **1** self-assembled as 150 nm micellar nanoparticles in water at ambient conditions and its hydrophobic pocket was capable of loading water insoluble dyes like Nile red. Dynamic light scattering techniques, electron and atomic force microscopes confirmed that the self-assembled structures exist in the form of spherical nanoparticles. Amphiphile **1** showed selective phase separation for anions such as sulfates and chlorides (salting-out) following the Hofmeister series. The Hofmeister effect of amphiphile **1** was explored for binding to anionic biomolecules ATP and its precursors ADP, AMP and Pi. Amphiphile **1** showed high preferential binding towards ATP over its precursors ADP, AMP and Pi. Isothermal calorimetric experiments further confirmed the ATP binding and it estimated three times higher binding constant for ATP towards amphiphile **1** as compared to Pi. Endothermic nature of the ATP binding to amphiphile **1** could provide advantages for selective binding at cancer tissue temperatures (42–44 °C), which are higher than normal tissues (37 °C). The thermo-responsive scaffold for ATP binding concept demonstrated here is not only restricted to the present example; in principle, this approach could be expanded to a wide range of other amphiphiles for future cancer treatment.

Conflicts of interest

The authors declare no competing financial interests.

Acknowledgements

The authors thank research grant from Department of Science and Technology (DST), New Delhi, INDIA, under nano-mission initiative project SR/NM/NS-42/2009. Smita thanks CSIR, New Delhi, India for research fellowship. The authors thank Dr Amitava Das at NCL-Pune for extending the ITC facilities for the present work, and Dr Harinath Chakrapani and Ms. Kavita Sharma of IISER-Pune for helping us with the cell viability data.

References

1 Y. Zhang and P. S. Cremer, *Proc. Natl. Acad. Sci. U. S. A.*, 2009, **106**, 15249–15253.
2 X. Chen, T. Yang, S. Kataoka and P. S. Cremer, *J. Am. Chem. Soc.*, 2007, **129**, 12272–12279.
3 H. I. Okur, J. Kherb and P. S. Cremer, *J. Am. Chem. Soc.*, 2013, **135**, 5062–5067.
4 P. L. Nostro and B. W. Ninham, *Chem. Rev.*, 2012, **112**, 2286–2322.
5 Y. Zhang and P. S. Cremer, *Annu. Rev. Phys. Chem.*, 2010, **61**, 63–83.
6 A. Salis and B. W. Ninham, *Chem. Soc. Rev.*, 2014, **43**, 7358–7377.
7 D. F. Parsons, M. Bostrom, P. L. Nostro and B. W. Ninham, *Phys. Chem. Chem. Phys.*, 2011, **13**, 12352–12367.

8 Y. Zhang and P. S. Cremer, *Curr. Opin. Chem. Biol.*, 2006, **10**, 658–663.
9 Y. Zhang, S. Furyk, D. E. Bergbreiter and P. S. Cremer, *J. Am. Chem. Soc.*, 2005, **127**, 14505–14510.
10 Y. Zhang, S. Furyk, L. B. Sagle, Y. Cho, D. E. Bergbreiter and P. S. Cremer, *J. Phys. Chem. C*, 2007, **111**, 8916–8924.
11 Y. Cho, Y. Zhang, T. Christensen, L. B. Sagle, A. Chilkoti and P. S. Cremer, *J. Phys. Chem. B*, 2008, **112**, 13765–13771.
12 J. Kherb, S. C. Flores and P. S. Cremer, *J. Phys. Chem. B*, 2012, **116**, 7389–7397.
13 K. B. Rembert, J. Paterova, J. Heyda, C. Hilty, P. Jungwirth and P. S. Cremer, *J. Am. Chem. Soc.*, 2012, **134**, 10039–10046.
14 H. Wei, S.-X. Cheng, X.-Z. Zhang and R.-X. Zhuo, *Prog. Polym. Sci.*, 2009, **34**, 893–910.
15 P. L. Nostro, B. W. Ninham, S. Milani, A. L. Nostro, G. Pesavento and P. Baglioni, *Biophys. Chem.*, 2006, **124**, 208–213.
16 J. Paterova, K. B. Rembert, J. Heyda, Y. Kurra, H. I. Okur, W. R. Liu, C. Hilty, P. S. Cremer and P. Jungwirth, *J. Phys. Chem. B*, 2013, **117**, 8150–8158.
17 J. P. Magnusson, A. Khan, G. Pasparakis, A. O. Saeed, W. Wang and C. Alexander, *J. Am. Chem. Soc.*, 2008, **130**, 10852–10853.
18 J. M. G. Swann, W. Bras, P. D. Topham, J. R. Howse and A. J. Ryan, *Langmuir*, 2010, **26**, 10191–10197.
19 L. Li, J.-H. Ryu and S. Thayumanavan, *Langmuir*, 2013, **29**, 50–55.
20 C. L. D. Gibb and B. C. Gibb, *J. Am. Chem. Soc.*, 2011, **133**, 7344–7347.
21 M. Qiu, S. Long, B. Li, L. Yan, W. Xie, Y. Niu, X. Wang, Q. Guo and A. Xia, *J. Phys. Chem. C*, 2013, **117**, 21870–21878.
22 P. K. Tarafdar, S. T. Reddy and M. J. Swamy, *J. Phys. Chem. B*, 2013, **117**, 9900–9909.
23 S. Manet, Y. Karpichev, D. Dedovets and R. Oda, *Langmuir*, 2013, **29**, 3518–3526.
24 B. A. Deyerle and Y. Zhang, *Langmuir*, 2011, **27**, 9203–9210.
25 E. M. Schwiebert and A. Zsembery, *Biochim. Biophys. Acta*, 2003, **1615**, 7–32.
26 W. G. Junger, *Nat. Rev. Immunol.*, 2011, **11**, 201–212.
27 A. Ohta, E. Gorelik, S. J. Prasad, F. Ronchese, D. Lukashev, M. K. K. Wong, X. Huang, S. Caldwell, K. Liu, P. Smith, J.-F. Chen, E. K. Jackson, S. Apasov, S. Abrams and M. Sitkovsky, *Proc. Natl. Acad. Sci. U. S. A.*, 2006, **103**, 13132–13137.
28 P. Pellagatti, L. Raffaghello, G. Bianchi, F. Piccardi, V. Pistoia and F. D. Virgillio, *PLoS One*, 2008, **3**, e2599.
29 L. M. Zheng, A. Ztchlinsky, C.-C. Liu, D. M. Ojcius and J. D.-E. Young, *J. Cell Biol.*, 1991, **112**, 279–288.
30 L. T. Wen and A. L. Knowles, *Br. J. Pharmacol.*, 2003, **140**, 1009–1018.
31 F. D. Virgillio, *Cancer Res.*, 2012, **72**, 5441–5447.
32 P. P. Neelakandan, M. Hariharan and D. Ramaiah, *Org. Lett.*, 2005, **7**, 5765–5768.
33 D. A. Jose, S. Mishra, A. Ghosh, A. Shrivastav, S. K. Mishra and A. Das, *Org. Lett.*, 2005, **9**, 1979–1982.
34 J. Kaur and P. Singh, *Chem. Commun.*, 2011, **47**, 4472–4474.
35 H. Jeon, S. Lee, Y. Li, S. Park and J. Yoon, *J. Mater. Chem.*, 2012, **22**, 3795–3799.
36 H. Wang and W.-H. Chan, *Org. Biomol. Chem.*, 2008, **6**, 162–168.
37 A. J. Moro, P. J. Cywinski, S. Korsten and G. J. Mohr, *Chem. Commun.*, 2010, **46**, 1085–1087.
38 Y. Zhou, Z. Xu and J. Yoon, *Chem. Soc. Rev.*, 2011, **40**, 2222–2235.
39 Z. Ge and S. Liu, *Chem. Soc. Rev.*, 2013, **42**, 7289–7325.
40 R. D. Issels, *Eur. J. Cancer*, 2008, **44**, 2546–2554.
41 G. Kong, R. D. Barun and M. W. Dewhirst, *Cancer Res.*, 2000, **60**, 4440–4445.
42 J. Fang, H. Nakamura and H. Maeda, *Adv. Drug Delivery Rev.*, 2011, **63**, 136–151.
43 K. Maruyama, *Adv. Drug Delivery Rev.*, 2011, **63**, 161–169.
44 P. S. Pramod, C. Katamura, S. Chapaker, N. Balasubramaniam and M. Jayakannan, *Biomacromolecules*, 2012, **13**, 3627–3640.
45 P. S. Pramod, R. Shah, C. Sonali, N. Balasubramanian and M. Jayakannan, *Nanoscale*, 2014, **6**, 11841–11855.
46 U. Sridhar, P. S. Pramod and M. Jayakannan, *RSC Adv.*, 2013, **3**, 21237–21241.
47 S. Kashyap and M. Jayakannan, *J. Phys. Chem. B*, 2012, **116**, 9820–9831.
48 S. Kashyap and M. Jayakannan, *J. Mater. Chem. B*, 2014, **2**, 4142–4152.
49 C. Wang, Q. Chen, Z. Wang and X. Wang, *Angew. Chem., Int. Ed.*, 2010, **49**, 8612–8615.
50 J. Liu, M.-a. Morikawa and N. Kimizuka, *J. Am. Chem. Soc.*, 2011, **133**, 17370–17374.
51 A. P. Borgan, W. R. Widger, D. Bensadek, I. R. Garcia, S. J. Gaskell and H. Kohn, *J. Am. Chem. Soc.*, 2005, **127**, 2741–2751.
52 B. Flachner, Z. Kovari, A. Varga, Z. Gugolya, F. Vonderviszt, G. N. Szabo and M. Vas, *Biochemistry*, 2004, **473**, 3436–3449.